# Orientation of the Phylloquinone Electron Acceptor Anion Radical in Photosystem I†

Fraser MacMillan,*,‡ Jonathan Hanley,‡ Louise van der Weerd,‡,§ Moritz Knüpling,‡,|| Sun Un,‡ and A. William Rutherford‡

*Section de Bioénergétique, Département de Biologie Cellulaire et Moléculaire, CNRS URA 2096, CEA Saclay, F-91191 Gif-sur-Yvette, France, Grenoble High Magnetic Field Laboratory, 25 Avenue de Martyrs, B.P. 166, F-38042 Grenoble, France, Department of Molecular Physics, Wageningen Agricultural University, NL-6703 Wageningen, The Netherlands, and Fachbereich Physik, Freie Universität Berlin, D-14195 Berlin, Germany*

*Received May 9, 1997; Revised Manuscript Received June 25, 1997*⊗

ABSTRACT: The photosynthetic reaction center of photosystem I (PS I) contains a phylloquinone molecule ($A_1$) which acts as a transient electron acceptor. In PS I from the cyanobacterium *Synechocystis* PCC 6803 under reducing conditions, we have photoaccumulated an EPR signal assigned to the phylloquinone radical anion. The phyllosemiquinone EPR spectrum has been studied in oriented multilayers of PS I using EPR at 9 GHz. In addition, the phyllosemiquinone spectrum has been obtained at 283 GHz using high-field, high-frequency EPR spectroscopy. From the orientation dependence of the spectrum at 9 GHz and the resolved g values obtained at 283 GHz, the phyllosemiquinone ring plane was determined to be almost perpendicular to the membrane (76°) while the oxygen−oxygen (O−O) axis of the quinone was found to make an approximate 63° angle to the membrane plane. The orientation of the ring plane is similar to that determined for the quinone electron acceptor ($Q_A$) in the purple bacterial reaction center, while the orientation of the O−O axis is significantly different. The new orientation information, when taken with data in the literature, allows the position of the phylloquinone in the reaction center to be better defined.

Photosystem I (PS I)[1] is a large multisubunit pigment−protein complex of approximately 300 kDa embedded in the photosynthetic membrane (for recent reviews, see refs 1 and 2). It is comprised of at least 11 different subunits and about 100 chlorophyll molecules. The general function of PS I is that of a light-driven plastocyanin/ferredoxin oxidoreductase. The redox components involved in the first steps of the photoinduced electron transfer are located in the reaction center core complex which is largely hydrophobic and is comprised of the subunits PsaA and PsaB. Upon light excitation, the primary electron donor, thought to be a dimer of chlorophyll *a* (chl *a*) molecules and known as $P_{700}$, forms a highly reducing singlet state, which consequently initiates charge separation between $P_{700}$ and the proposed primary acceptor $A_0$, a chl *a* molecule. An electron is then transferred to a molecule of phylloquinone, known as $A_1$, and subsequently through a series of iron−sulfur centers labeled $F_X$, $F_A$, and $F_B$.

The first evidence of two intermediate electron transfer components between $P_{700}$ and $F_X$ came from the observation of two distinct EPR spectra following progressively longer periods of illumination at temperatures around 200 K under reducing conditions (*3*, *4*). While several lines of evidence have indicated that a phylloquinone is the electron carrier $A_1$ in PS I (reviewed in ref 2), it has only recently been accepted that the semiquinone constitutes one of the EPR signals that are generated by photoaccumulation (*5*) (see also ref 6).

The three-dimensional structure of PS I in the cyanobacterium *Synechococcus elongatus* has been determined at a resolution of 4.0 Å (*7*). However, the location of the phylloquinone has proven to be difficult to determine within the electron density map owing to its relatively small size and its structural similarity to aromatic amino acid side chains. In the present work, through the use of oriented multilayers of PS I from *Synechocystis* PCC 6803 and EPR spectroscopy, we have determined the orientation of the phylloquinone ring plane and the oxygen−oxygen (O−O) axis relative to the membrane.

## MATERIALS AND METHODS

Liquid cultures of wild type *Synechocystis* PCC 6803 were grown in BG11 medium (*8*), buffered with HEPES (6 mM at pH 7.3). Cells in liquid culture were grown to an OD (820 nm) of approximately 1.5 and then harvested by centrifugation. The cells were broken by French press, and the cell debris was removed by further centrifugation.

† This work was supported by grants from the Human Capital and Mobility Network programme (HCM Grant ERBCHRXCT940524), a European Union Training and Mobility of Researchers personal fellowship (TMR Grant ERB4001GT957977 to F.M.), and the Human Frontiers Science Programme (HFSPO Grant RGO349).

* To whom correspondence should be addressed. Fax: + 33 1 69 08 87 17.

‡ CNRS URA 2096.

§ Wageningen Agricultural University.

|| Freie Universität Berlin.

⊗ Abstract published in *Advance ACS Abstracts,* August 1, 1997.

[1] Abbreviations: $A_0$, primary electron acceptor in PS I, chlorophyll *a*; $A_1$, secondary electron acceptor in PS I, phylloquinone (vitamin $K_1$); BDPA, α,γ-bidiphenylene-β-phenylallyl; DPPH, α,α′-diphenyl-β-picryl hydroyl; β-DM, *n*-dodecyl β-D-maltoside; EDTA, ethylenediaminetetraacetic acid; EPR, electron paramagnetic resonance; ENDOR, electron nuclear double resonance; $F_A$, $F_B$, and $F_X$, three [4Fe-4S] centers of PS I; HEPES, *N*-2-(hydroxyethyl)piperazine-*N*′-2-ethanesulfonic acid; hfc, hyperfine coupling constant; MES, 2-(*N*-morpholino)ethanesulfonic acid; OD, optical density; PS I, photosystem I; PsaA, B, C, ..., polypeptides coded by the genes *psa*A, -B, -C, ..., respectively; Tricine, *N*-[2-hydroxy-1,1-bis(hydroxymethyl)ethyl]glycine.

S0006-2960(97)01097-0 CCC: $14.00 

The isolated membranes were washed at 4 °C four times with Tricine (20 mM at pH 7.8), potassium chloride (10 mM), and EDTA (1 mM). PS I particles were isolated by solubilization with $\beta$-DM [1% (w/v)] and purified on a sucrose density gradient as described in ref 9. Both the upper green band, consisting of highly enriched monomeric PS I particles, and the lower green band, consisting of trimeric PS I particles, were dialyzed against Tricine/NaOH (20 mM at pH 7.8) containing $\beta$-DM [0.04% (w/v)] and concentrated by ultrafiltration (Centriprep 100, Amicon). All samples were stored at −80 °C until they were used.

In order to prepare the samples for orientation, membrane fragments and PS I trimers were further dialyzed (4 °C) for 48−72 h against Tricine (20 mM at pH 8.0), collected by centrifugation, and resuspended in distilled $H_2O$. They were then spread onto mylar sheets and allowed to dry for 2−4 days against a relative humidity of 80% at 4 °C (*10*) (see also ref 11).

For frozen solution EPR samples, membrane fragments were put in standard Suprasil quartz EPR tubes (outside diameter of 4 mm). The iron−sulfur centers $F_A$ and $F_B$ were fully reduced by the addition of sodium dithionite (25 mM) in glycine (200 mM at pH 10.0) followed by dark adaptation (15 °C for 30 min). Brief periods of illumination were given at variable temperatures (in cooled ethanol, 200−240 K). Illumination was performed using an 800 W lamp with a 4 cm water filter and a 720 nm cutoff filter. Samples were then dark-adapted (2 min) at 200 K before cooling to 77 K and transfer in the dark to the spectrometer.

Oriented membrane fragments on two mylar sheets were placed in EPR tubes and iron−sulfur centers $F_A$, $F_B$, and $F_X$ fully reduced by the addition of sodium dithionite (50 mM) in glycine (final concentration of 200 mM at pH 10.0) followed by a brief (1 min) period of illumination at 200 K in a solid $CO_2$/ethanol bath. The samples were mounted in the EPR cavity on a home-built goniometer. The angles given in the Results are the magnetic field relative to the plane of the mylar sheets. In order to prepare samples with the phylloquinone reduced, the samples were illuminated at 220 K (3 min) which results in the following state, $P_{700}A_0A_1^-F_A^-F_B^-F_X^-$. The EPR signals of the phyllosemiquinone, the reduced iron−sulfur centers, and $^3P_{700}$ were recorded at different orientations (in 10° steps) relative to the magnetic field.

X-Band EPR spectra were measured on a Bruker ESP300 spectrometer. A standard rectangular Bruker EPR cavity (ER4102T) equipped with an Oxford helium (ESR 900) cryostat was used. The microwave frequency was measured using a Hewlett-Packard (HP5350B) frequency counter. The magnetic field was measured using a Bruker gaussmeter (ER035M). The measured *g* values were corrected for an offset against a known *g* standard (DPPH).

The influence of the mylar sheets in the magnetic field was determined using a sample (BDPA, Sigma) which has essentially no measurable *g* anisotropy. The shift in the microwave frequency observed when the sample was rotated corresponded to a variation of the observed *g* value of ±0.00005 which is much smaller than the effects observed in this paper.

The high-field EPR setup has been described previously (*12*). However, in the present work, the microwave source was a 95 GHz Gunn diode used together with a tripler to generate the high measuring frequency. Spectra were recorded at 283 GHz and 10 K. The samples were the same as those used for the frozen solution measurements at 9 GHz (see above).

The powder spectrum and oriented spectra obtained were simulated using the procedure outlined in ref 13. Electron spin operators of second-order or higher were ignored. This results in a spin Hamiltonian matrix which is composed of two 2 × 2 submatrices, which describe each of the two electron spin manifolds. The submatrices were solved analytically assuming that the nuclear Zeeman interactions were isotropic. No assumptions about the relative orientation of the hyperfine and **g** tensors were made. Both the nominally allowed and forbidden transition probabilities were calculated. The relative orientation of the hyperfine tensors and the *g* axis system were taken from ENDOR data (ref 14 and F. MacMillan et al., unpublished results).

For the powder spectrum, powder averaging was accomplished by random generation of 500−1000 orientations of the magnetic field with respect to the **g** tensor reference frame, followed by calculation of the spectrum for the given orientation and summation over all the orientations. As the hyperfine couplings were unresolved in the high-field spectrum, it was sufficient to fit numerically this spectrum using only the *g* anisotropy and single isotropic Gaussian line-broadening parameter. Numerical fitting involved minimization of the squared difference of the experimental and calculated spectra using standard techniques (*15*).

For oriented spectra, an intermediate reference frame (IRF) was used. The IRF *z* axis was along the membrane perpendicular. The *x* and *y* directions are orthogonal to the *z* axis. The angle measured during the experiment describes the angle between the magnetic field and the IRF *z* axis. Three Euler angles describe the relative orientation of the *g* axis with respect to the IRF. Two of these Euler angles describe the orientation of the *g* axis system relative to the *z* axis of the intermediate axis system. In this paper, angles are reported as pairs, where the second describes a rotation of the *g* axis system about the IRF *z* axis followed by a rotation about the IRF *y* axis. Orientation averaging was achieved by generating 500−1000 random orientations of the magnetic field in the *x*−*y* plane of the IRF while maintaining a fixed angle between the magnetic field and the *z* axis. The averaging process, in effect, averages all possible values of the third Euler angle, and therefore, the oriented spectra are independent of this angle. To obtain the orientation of the *g* axis system relative to the IRF *z* axis, and hence the membrane plane normal, six oriented spectra taken at different magnetic field membrane plane angles were simultaneously fitted using standard conjugate gradient minimization techniques (*15*). The 9 GHz orientation spectra were fitted using the relative *g* value (i.e. relative to the orientation-dependent shift). Since the fits were essentially independent of the absolute *g* value, any experimental uncertainty with respect to the absolute field calibration was accounted for.

## RESULTS

Figure 1A shows a plot of the yield of photoaccumulated EPR signals measured at 20 K (determined by double integration of the EPR signal) versus the length of time that the sample had been illuminated at three different temperatures. In addition, the bold, horizontal line represents the maximum yield of $P_{700}^+$ generated by freezing under illumination of a sample with a concentration and size identical to that used for the investigation of the signals

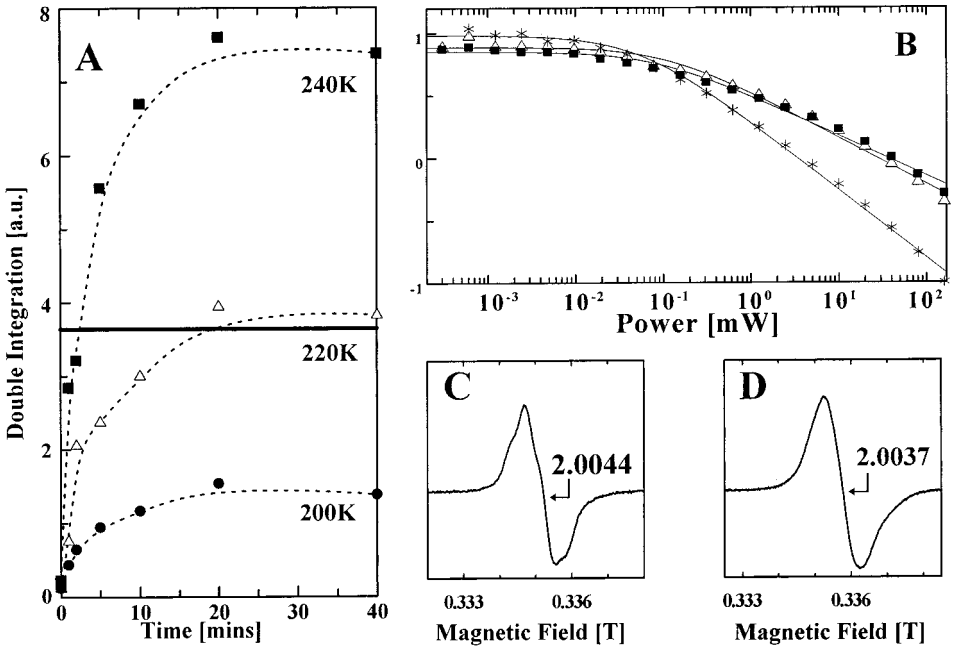


FIGURE 1: (A) Intensities of the EPR signals (detemined by double integration of the signal) plotted against the time of illumination at three different temperatures. See Materials and Methods for sample details. The solid horizontal line is the maximum yield of $P_{700}^+$. Filled circles are after 200 K, open triangles after 220 K, and filled squares after 240 K illumination. (B) Progressive microwave power saturation of the intensity of the EPR signal of reduced PS I after 220 K illumination for 40 min (△) and after 240 K illumination for 40 min (■) and of $P_{700}^+$ (*). The continuous lines are fits using the equation $I = (1 + P/P_{1/2})^b$, where $P$ is the microwave power. $P_{1/2}$ ($A_1^-$) = 0.113. $P_{1/2}$ ($A_1^-/A_0^-$) = 0.082. $P_{1/2}$ ($P_{700}^+$) = 0.054. (C) EPR spectrum of *Synechocystis* PCC 6803 membrane fragments under reducing conditons after illumination at 220 K for 40 min. Panel D is like panel C but after illumination at 240 K for 40 min. Experimental conditions were as follows: microwave power ($P_{MW}$), 0.1 mW; field modulation amplitude, 0.2 mT; accumulation time, 160 s; and $T$ = 20 K.

photoaccumulated under reducing conditions. Further illumination at low temperatures (10 K) resulted in no further increase in the $P_{700}^+$ signal amplitude, and this is therefore taken as an estimate of one spin per PS I reaction center.

Illumination of a reduced sample at 200 K resulted in an EPR signal (Figure 1C) with partially resolved hyperfine coupling and with a *g* value of 2.0044. Such *g* values are characteristic of quinones (see also the discussion of high-field results below and refs 16−18). The time course of illumination (Figure 1A, filled circles) indicates however that only about 40% of this signal is photoaccumulated relative to $P_{700}^+$. After illumination at 220 K (open triangles) for 20 min, the EPR signal increased to approximately one spin per PS I. The *g* value and line shape of the signal were the same as those of the signal generated at 200 K, and they did not change during the course of the photoaccumulation procedure (not shown).

At 240 K (filled squares), the yield of the photoaccumulated signal increased and reached approximately two spins per $P_{700}$ after 20 min of illumination. This additional spin was also correlated with a shift in the observed *g* value (from 2.0044 to 2.0037) and an asymmetric broadening of the EPR signal (Figure 1D). These results indicate that two different radical species per $P_{700}$ were photoaccumulated under these conditions. The second species (obtained by spectral subtraction, data not shown) has a lower *g* value ($g \approx 2.0028$) and a broader EPR line width (∼10 G) characteristic of a chlorophyll anion radical (see ref 19) and is attributed to the chlorophyll electron acceptor anion $A_0^-$. The results obtained here in *Synechocystis* PCC 6803 are comparable to those previously observed in plant PS I (*3, 4*). They also confirm that no gradual reduction of the phyllosemiquinone to the quinol occurs at 220 K. We also noted an apparent loss of resolution of the hyperfine lines from $A_1^-$ in the $A_1^- + A_0^-$ spectrum (Figure 1D). This may originate from a magnetic interaction between the two radicals, indicative of their close proximity.

The microwave saturation ($P_{1/2}$) of each signal was measured at 20 K (Figure 1B). As can be seen, the different signals saturate differently and thus the spin quantification determined using a microwave power of 0.1 mW was done under slightly saturating conditions. This results in an underestimation of the amounts of radicals generated. The saturation effect (estimated from the fits in Figure 1B) is different in each sample (ca. 12−25%). If this is taken into account, the relative yields of the radicals generated at 200, 220, and 240 K are 36, 92, and 180%, respectively.

It has been previously reported that it is possible to photoaccumulate several radical species (up to a maximum of four) per $P_{700}$ in spinach PS I particles (*20*). However, under the conditions employed in the present study, the reduction of only two species per $P_{700}$ was observed in *Synechocystis*. This apparent discrepancy may be due to a species difference and could be related to the very different electron donation rates to $P_{700}$ from their natural electron donors in the two species (*21*). Such differences could have a significant influence on the photoaccumulation experiment.

In order to minimize contributions from the chlorophyll anion radical signal, all the further investigations of the phyllosemiquinone in this paper employed an illumination time of ∼3 min at 220 K which should result in the formation of less than the maximum yield of phyllosemiquinone radical (Figure 1A). Figure 2A shows the EPR spectrum at 9 GHz of the phyllosemiquinone from *Synechocystis* PCC 6803 membrane fragments generated under these conditions. The spectrum shows a partially resolved structure which results from the **g** tensor and by hyperfine interactions. In oriented samples, the change in the position of the zero crossing of the signal (*22*) can be used to determine the orientation of

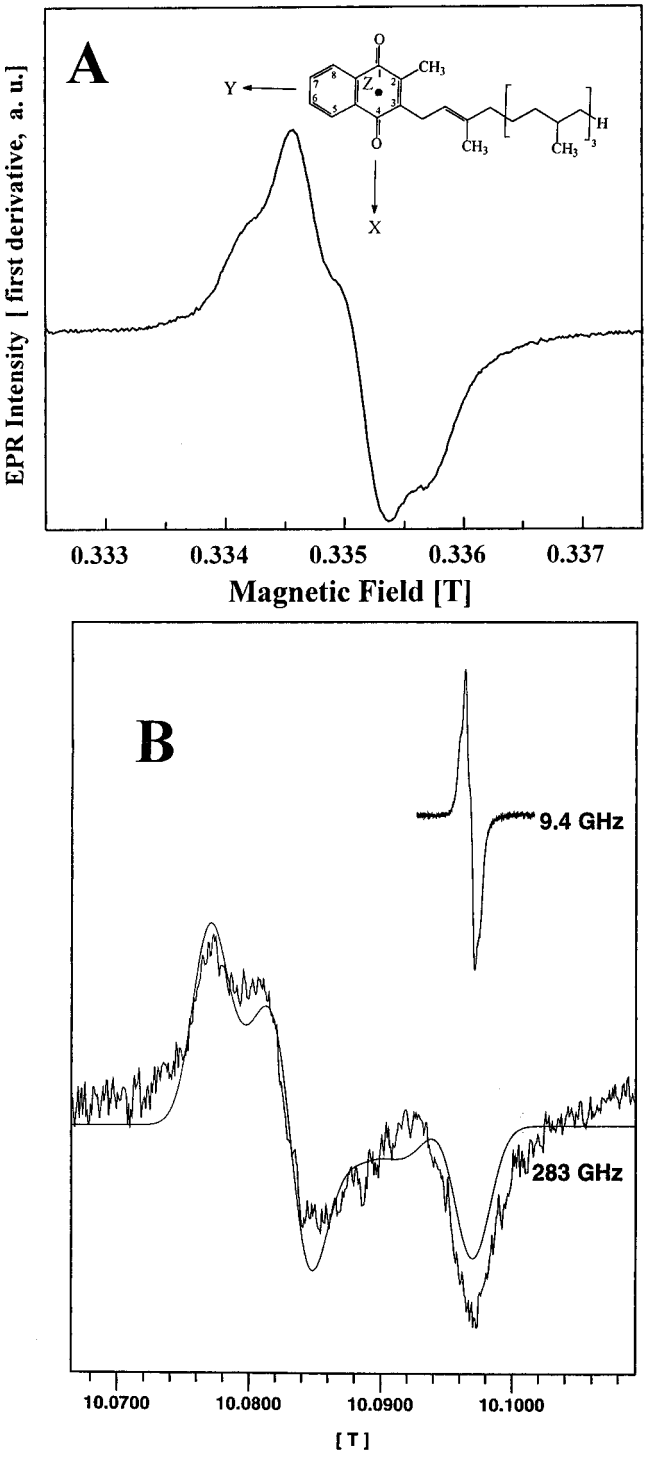


FIGURE 2: (A) 9 GHz EPR spectrum of the phyllosemiquinone in *Synechocystis* PCC 6803 membrane fragments. Dark-adapted samples treated with dithionite (for details, see the text) after illumination at 220 K for 3 min. Experimental conditions were as follows: $P_{MW}$, 0.1 mW; field modulation amplitude, 0.2 mT; accumulation time, 160 s; and $T = 20$ K. (Inset) Structural formula and numbering scheme including the **g** tensor axis for vitamin $K_1$ ($VK_1$, 2-methyl-5-phytyl-1,4-naphthoquinone). (B) 9 GHz (0.3 T) and 283 GHz (10.1 T) spectra of phyllosemiquinone in *Synechocystis* PCC 6803 membrane fragments. Sample treatment as in Figure 1. The 283 GHz spectrum was obtained at 10 K using 0.15 mT and a 10 kHz field modulation. The calculated spectrum is shown using the **g** tensor (Table 1) and an isotropic 20 G line width.

the semiquinone ring plane due to the magnitude of the $g$ anisotropy even at X-band (*16*).

Previously, data on oriented multilayers of PS I were obtained for samples in membranes and isolated protein

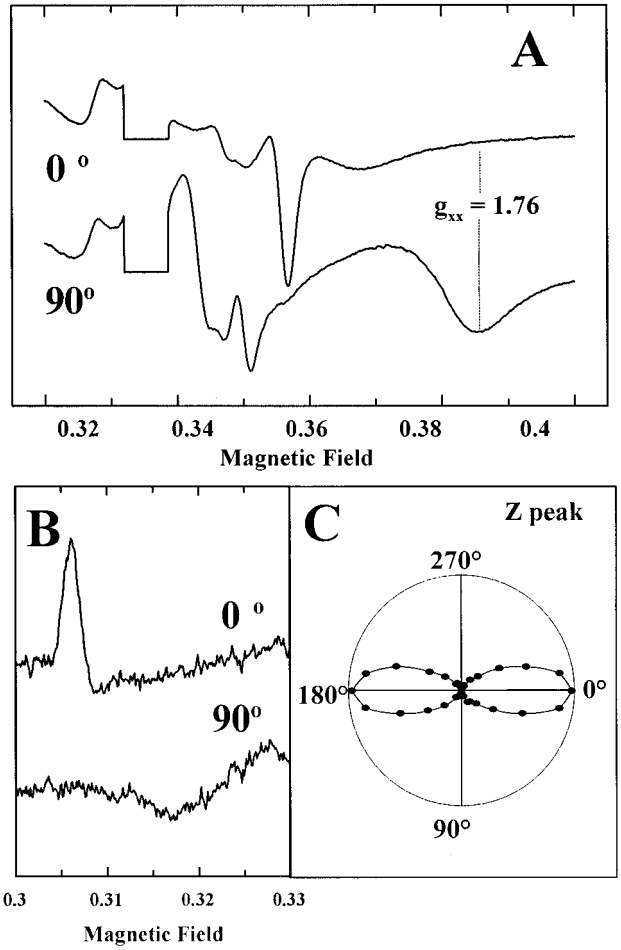


FIGURE 3: (A) EPR signals of the reduced iron−sulfur centers at 0 and 90° in partially dried PS I trimers isolated using $\beta$-DM. Two mylar sheets were submerged in a 20% (w/v) sodium dithionite [200 mM glycine/NaOH buffer (pH 8)] and incubated for 15 min in darkness before freezing (for details, see the text). Experimental conditions were as follows: $P_{MW}$, 10 mW; field modulation frequency, 100 kHz; field modulation amplitude, 1.0 mT; accumulation time, 160 s; and $T = 8$ K. (B) Low-field $g_{zz}$ peak of the light-induced EPR triplet of $P_{700}$ at 0 and 90°. The sample was prepared as above (see the text for details). The triplet was induced by continuous illumination at 5 K. The spectra are light minus dark spectra. Experimental conditions were as follows: $P_{MW}$, 0.08 mW; field modulation frequency, 100 kHz; field modulation amplitude, 2.0 mT; accumulation time, 80 s; and $T = 4$ K. (C) Polar plot of the orientation dependence of the low-field $g_{zz}$ peak of the light-induced EPR triplet of $P_{700}$.

complexes (*10*, *23*−*26*). In the present work, PS I trimers and membrane fragments were used. Thus, it was important to establish that they also demonstrated the same orientation behavior as had been previously reported. Complete data sets for the EPR signals of the phyllosemiquinone, the reduced iron−sulfur centers, and $^3P_{700}$ were recorded at different orientations (in 10° steps). Figure 3 shows two orientations for the reduced iron−sulfur centers at 8 K. Their ordering is confirmed by the very striking orientation-dependent changes of the iron−sulfur center EPR signals. The peak at $g = 1.76$, attributed to the $g_{xx}$ component of $F_X$ (Figure 3A), is at a maximum when the membrane is perpendicular to the magnetic field as previously reported (*10*, *25*). In ref 10, it was also demonstrated, using oriented isolated PS I particles from spinach, that the $g_{zz}$ component of the $^3P_{700}$ state was at a maximum when the membrane is parallel to the magnetic field. This indicated that the plane of the $P_{700}$ tetrapyrol ring is perpendicular to the membrane. As shown in Figure 3B, the same result is obtained here

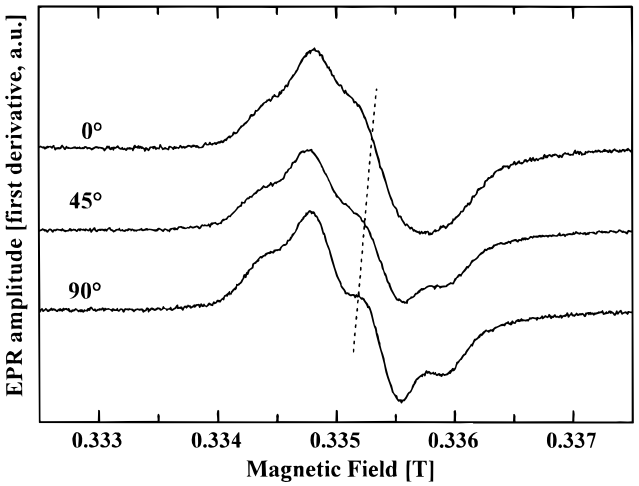


FIGURE 4: Orientation dependence of the phyllosemiquinone EPR signal at 9 GHz. For sample preparation, see previous figures and text. The angle of the mylar sheet relative to the magnetic field is indicated. The dotted line indicates the peak maxima of the integrated spectra. Experimental conditions were as follows: $P_{MW}$, 0.005 mW; field modulation frequency, 100 kHz; field modulation amplitude, 0.1 mT; accumulation time, 160 s; and $T = 26$ K.

using *Synechocystis* PS I particles. A polar plot of the orientation of the low-field $g_{zz}$ component of the $^3P_{700}$ state is also shown (Figure 3C). These similarities demonstrate clearly but not surprisingly that the $P_{700}$ in *Synechocystis* PS I has the same orientation as that observed in PS I from plants. All the observed orientation dependencies indicate that the isolated RCs of *Synechocystis* are well-ordered and have the same orientation as seen previously.

Figure 4 shows EPR spectra of $A_1^-$ detected in PS I multilayers oriented at 0, 45, and 90° relative to the magnetic field. These spectra show marked orientation dependencies which are manifested as changes in the line shape and *g* value. The shape of an EPR signal is determined by the **g** tensor and also by hyperfine interactions, both of which are orientation-dependent. As an approximation, however, the hyperfine interactions are symmetrical about the field position. Thus, the only parameter that determines the zero crossing of the EPR line is the *g* anisotropy. Here, we observe that the phyllosemiquinone *g* value (defined as the zero crossing of the first derivative line) varies with the orientation of the sample with respect to the magnetic field.

In order to obtain more precise information regarding the phylloquinone orientation, an accurate determination of the **g** tensor is required. Figure 2B shows 283 GHz spectra of phyllosemiquinone. To illustrate the resolution gained at this frequency, the 9 GHz spectrum has been plotted on a comparable scale. Although the signal to noise ratio is poorer than at X-band, the *g* anisotropy is clearly resolved. The principal *g* values of the phyllosemiquinone determined by simulation of the 283 GHz spectrum (Figure 2B, smooth line) and those of the isolated phyllosemiquinone anion radical ($VK_1^-$) generated in a frozen alcoholic solution (*17*, *27*) are given in Table 1. The absolute accuracy of the *g* values is $\pm 2.0 \times 10^{-4}$, reflecting the lack of an internal *g* standard and the technical problems related to magnet calibration and control. The relative accuracy of the *g* values is at least 1 order of magnitude more; hence, the extent of anisotropy, as measured by $g_{xx} - g_{zz}$, is accurate to within $\pm 2.0 \times 10^{-5}$. The orientation of the *g* axis system relative to the molecular frame for semiquinones has been determined

Table 1: Principal Values of the **g** Tensors of the PS I Electron Acceptor Radical Anion $A_1^{\bullet -}$ and of the Vitamin $K_1$ ($VK_1^{\bullet -}$) Radical Anion in a Frozen Alcoholic Solution

| radical | $g_{xx}$ | $g_{yy}$ | $g_{zz}$ | $^1/_3$ Tr $g^a$ |
|---|---|---|---|---|
| $A_1^{\bullet -}$ [b] | 2.006 25 | 2.005 03 | 2.002 27 | 2.004 52 |
| $VK_1^{\bullet -}$ [c] | 2.005 66 | 2.004 93 | 2.002 16 | 2.004 25 |
| $VK_1^{\bullet -}$ [d] | 2.005 88 | 2.004 96 | 2.002 25 | 2.004 36 |

[a] $^1/_3$ Tr $g = {}^1/_3(g_{xx} + g_{yy} + g_{zz})$. [b] This work; values obtained by simulation of the powder (283 GHz) EPR spectra. Absolute error is $\pm 2 \times 10^{-4}$. Relative error is $\pm 2 \times 10^{-5}$. [c] W-band (95 GHz) EPR measurements (*17*); error is $\pm 5 \times 10^{-5}$. [d] D-band (132 GHz) EPR measurements (*27*).

in ref 17. The $g_{zz}$ is perpendicular to the ring plane, while $g_{xx}$ is along the C−O bond direction.

Until now, the only other **g** tensor data for the photoaccumulated phyllosemiquinone obtained by EPR at frequencies higher than 9 GHz were taken at 35 GHz (ref 28 and F. MacMillan et al., unpublished results). However, at 35 GHz, the resolution of the *g* anisotropy is still masked by hyperfine interactions. At the magnetic field (∼10 T) used here in the high-frequency EPR experiment, the magnitudes of the hyperfine interactions negligible relative to the *g* anisotropy, and thus, the accuracy of the observed **g** tensor is much greater.

Recently, *g* values for $A_1^-$ were deduced from simulations of the electron spin-polarized (ESP) $P_{700}^+A_1^-$ radical pair signal measured at 95 GHz (*29*). These values are quite close to those measured here and can be taken as evidence that the photoaccumulated species is the same as that involved in the transiently detected radical pair.

By combining the *g* values determined by the high-field EPR experiments with spectra obtained from oriented samples at 9 GHz, it is possible to obtain the orientation of the phyllosemiquinone relative to the membrane surface. Figure 5 shows two spectra of the radical taken at different tilt angles with respect to the magnetic field. For simplicity, only the quartet hyperfine coupling [taken from ENDOR data (*14*) and F. MacMillan et al., unpublished results] from the methyl group at position 2 (see the inset in Figure 2A) and a single small (3 MHz) isotropic hyperfine coupling were considered in the calculation. In Figure 5, there appears to be a systematic error in the fitting. As the entire width of spectrum is accounted for by the large quartet coupling of the methyl group, the error seems not to arise from the neglect of any larger hyperfine interactions but rather from the use of a single small isotropic hyperfine coupling instead of the many that are measured by ENDOR spectroscopy (F. MacMillan et al., unpublished results).

The best fit to the experimental spectra occurs for the Euler angles 76 and 63°. The semiquinone O−O axis (defined as the $g_{XX}$ direction of the **g** tensor; see the inset in Figure 2A) is tilted about 63° with respect to the membrane plane, and the quinone ring plane is oriented at ∼76° to the membrane plane. A simple error analysis was carried out by plotting the combined squared-residual of six simultaneously simulated spectra as a function of the two Euler angles (see Materials and Methods). A conservative error margin for the six-spectrum fit is ±10° in both directions. This orientation is also represented pictorially in Figure 5.

## DISCUSSION

By using EPR spectra at 9 GHz of oriented samples in combination with accurate *g* values obtained using high-field

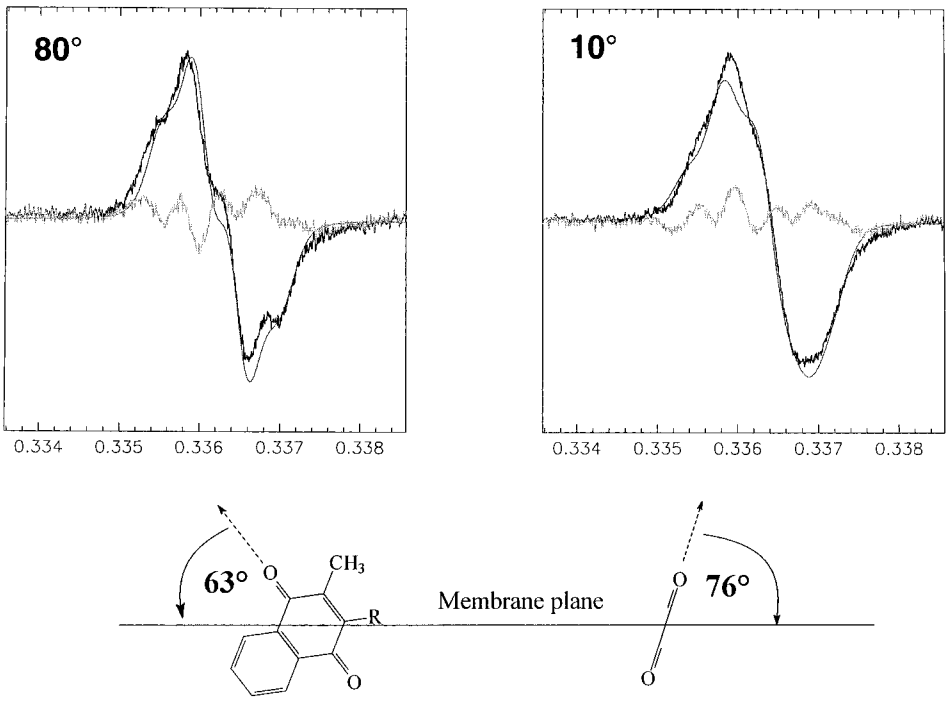


FIGURE 5: (Top) Two of the six simultaneously fitted oriented spectra (see the text for details) used to obtain the orientation of the **g** axis system relative to the IRF *z*-axis. The small resulting residual is also shown in gray. (Bottom) Two schematic representations (frontal and side view) of the orientation of the radical anion with respect to the membrane plane.

EPR at 283 GHz, the orientation of the ring plane and the O−O axis of the phyllosemiquinone, $A_1^-$, have been determined (see Figure 5). This information can be added to current structural models of PS I. In addition, earlier studies have provided some information which, taken with the present results, may in principle allow the position of $A_1$ to be better defined.

Simulations of the ESP $P_{700}^+A_1^-$ radical pair signal at 24 and 95 GHz indicated that the O−O axis of the quinone was roughly parallel to the vector joining $P_{700}$ and $A_1$ (*29*−*31*). Similar conclusions were drawn from the analysis of quantum beats in 9 GHz EPR transients (*32*, *33*). Given the expectation that the $P_{700}-A_1$ vector is oriented a few tens of degrees away from being perpendicular to the membrane, then the present finding that the O−O axis is tilted at ∼63° to the membrane is consistent with these kinetic EPR studies.

The combination of the ∼63° tilt of the O−O axis (reported here) taken together with this axis being parallel to the $P_{700}-A_1$ vector (see above) leads to the conclusion that the $P_{700}-A_1$ vector is tilted by ∼63° relative to the membrane plane. In the purple bacterial reaction center, the $P-Q_A$ axis is tilted by ∼70° to the membrane plane (e.g. ref 34). This may indicate that $A_1$ is somewhat laterally shifted as compared to the position of $Q_A$; however, only slight differences in the measured angles could allow $A_1$ to occupy a position equivalent to that of $Q_A$ in the bacterial reaction center. The combined errors in the measured angles are probably sufficient to allow for this situation.

The PS I reaction center is structurally related to that of purple bacteria (*7*, *35*); however, several obvious structural differences exist, and these reflect functional differences. At the level of the quinone acceptors, the orientation of the ring plane reported here is similar to that of $Q_A$. In contrast, the O−O axis for $A_1$ is found to be approximately ∼63° rather than ∼10° for $Q_A$ in the bacterial reaction center (e.g. ref 34). In addition, the $P_{700}-A_1$ distance [25.4 Å (*36*)] appears to be a few angstroms shorter than the $P-Q_A$ distance in the purple bacterial reaction center. We have tried to envisage what could be the minimum change in the positioning of $Q_A$ that would shift it to give a position that would account for the spectroscopic data available for $A_1$. Given that $Q_A$ has a hydrogen bond to each of its carbonyl groups and these seem to hold the O−O axis close to parallel to the membrane, then one such change would be to remove the hydrogen bond proximal to the central $C_2$ axis of the reaction center and to swing the quinone further into the membrane while leaving the distal hydrogen bond intact. By this minor adjustment, when the O−O angle versus the membrane is changed to approximately 60−65°, the $P_{700}-A_1$ distance is decreased by approximately 3 Å. We speculate that a change structurally equivalent to that described above (or perhaps more likely the reverse of such a change) could have occurred during the course of the evolutionary events that separate the two types of reaction centers from their common ancestor (see ref 37).

An estimate of the position of $A_1$ in the reaction center can be obtained when the orientation data in the present work (∼63° between the O−O axis and the membrane plane) are combined with the following recently published spectroscopic results. (1) The $P_{700}-A_1$ distance is 25.4 Å (*36*). (2) The $P_{700}-A_1$ vector is close to parallel to the O−O axis of the quinone (*29*). (3) The $P_{700}-F_X$ distance is 32 Å, and its vector is close to perpendicular to the membrane (*7*). By simple geometric considerations, $A_1$ is predicted to be located on the circle 14.2 Å from $F_X$. The errors in the estimated angles discussed above make this distance only an approximation.[2] The analogy to the bacterial reaction center

[2] While this work was under review, there were three reports (by R. Bittl, by D. Stehlik, and by Y. Deligiannakis, J. A. Hanley, and A. W. Rutherford at a symposium on Current Topics on Structure and Function of Oxygenic Photosynthesis in Berlin, Germany) of experimental evidence on the position of $A_1$. These new data provide us with more confidence in this estimate.

discussed in the previous paragraph may provide further constraints on the location of $A_1$.

Another major difference between the $Q_A$ of the bacterial reaction center and the phylloquinone $A_1$ in PS I is that $A_1$ has a functional midpoint potential which is estimated to be 800 mV lower than that of phylloquinone in solution, while for $Q_A$ (a menaquinone) in *Rhodopseudomonas viridis*, the potential is close to that of the isolated menaquinone. It has been shown that the *g* values, and particularly the $g_{xx}$ of quinones and tyrosine radicals, reflect their electrostatic environments (*17*, *38*). Comparison of the measured *g* values of $A_1^-$ with those of the $VK_1$ anion (Table 1) shows that, while the $g_{yy}$ and $g_{zz}$ values are similar to those of $VK_1^-$ in solution, the $g_{xx}$ value of $A_1^-$ is significantly larger. This is taken as an indication that $A_1^-$ exists in a negative electrostatic environment. This could be responsible for the unusually low midpoint potential of $A_1$. Similar arguments have been recently made on the basis of the *g* values obtained from the ESP-ESR signal of the $P_{700}^+A_1^-$ radical pair at 95 GHz (*29*).

## ACKNOWLEDGMENT

Robert Bittl and Art van der Est are thanked for communication of their results prior to publication.

## REFERENCES

1. Golbeck, J. H., and Bryant, D. A. (1991) in *Current Topics in Bioenergetics* (Lee, C. P., Ed.) Vol. 16, pp 83−177, Academic Press, Inc., San Diego.
2. Brettel, K. (1997) *Biochim. Biophys. Acta 1318*, 322.
3. Gast, P., Swarthoff, T., Ebskamp, F. C. R., and Hoff, A. J. (1983) *Biochim. Biophys. Acta 722*, 163.
4. Bonnerjea, J. R., and Evans, M. C. W. (1982) *FEBS Lett. 148*, 313.
5. Heathcote, P., Moënne-Loccoz, P., Rigby, S. E. J., and Evans, M. C. W. (1996) *Biochemistry 35*, 6644.
6. Itoh, S., Iwaki, M., and Ikegami, I. (1987) *Biochim. Biophys. Acta 893*, 508.
7. Krauss, N., Schubert, W. D., Klukas, O., Fromme, P., Witt, H. T., and Saenger, W. (1996) *Nat. Struct. Biol. 3*, 965.
8. Rippka, R., Deruelles, J., Waterbury, J. B., Herdmann, M., and Stanier, R. Y. (1979) *J. Gen. Microbiol. 111*, 1.
9. Rögner, M., Nixon, P. J., and Diner, B. A. (1990) *J. Biol. Chem. 265*, 6189.
10. Rutherford, A. W., and Sétif, P. (1990) *Biochim. Biophys. Acta 1019*, 128.
11. Blasie, J. K., Erecinska, M., Samuels, S., and Leigh, J. S. (1978) *Biochim. Biophys. Acta 501*, 22.
12. Muller, F., Hopkins, M. A., Coron, N., Grynberg, M., Brunel, L. C., and Martinez, G. (1989) *Rev. Sci. Instrum. 60*, 3681.
13. Abragam, A. (1961) *Principles of Nuclear Magnetism*, pp 167−178, Oxford University Press, Oxford.
14. Rigby, S. E. J., Evans, M. C. W., and Heathcote, P. (1996) *Biochemistry 35*, 6651.
15. Press, W. H., Flannery, B. P., Teukolsky, S. A., and Vetterling, W. T. (1988) in *Numerical Recipies*, Cambridge University Press, New York.
16. Hales, B. J., and Case, E. E. (1981) *Biochim. Biophys. Acta 637*, 291.
17. Burghaus, O., Plato, M., Rohrer, M., Mobius, K., MacMillan, F., and Lubitz, W. (1993) *J. Phys. Chem. 97*, 7639.
18. MacMillan, F., Lendzian, F., and Lubitz, W. (1995) *Magn. Reson. Chem. 33*, S81.
19. Lubitz, W. (1991) in *Chlorophylls* (Scheer, H., Ed.) pp 903−944, CRC Press, Boca Raton, FL.
20. Heathcote, P., Hanley, J. A., and Evans, M. C. W. (1993) *Biochim. Biophys. Acta 1144*, 54.
21. Hervás, M., Ortega, J. M., Navarro, J. A., De la Rosa, M. A., and Bottin, H. (1994) *Biochim. Biophys. Acta 1184*, 235.
22. Tiede, D. M., and Dutton, P. L. (1981) *Biochim. Biophys. Acta 637*, 278.
23. Prince, R. C., Crowder, M. S., and Bearden, A. (1980) *Biochim. Biophys. Acta 592*, 323.
24. McCracken, J. L., and Sauer, K. (1983) *Biochim. Biophys. Acta 724*, 83.
25. Hootkins, R., and Bearden, A. (1983) *Biochim. Biophys. Acta 723*, 16.
26. Guigliarelli, B., Guillaussier, J., More, C., Sétif, P., Bottin, H., and Bertrand, P. (1993) *J. Biol. Chem. 268*, 900.
27. Bowman, M. K., Thurnauer, M. C., Norris, J. R., Dikanov, S. A., Gulin, V. I., Tyryshkin, A. M., Samoilova, R. I., and Tsvetkov, Yu. D. (1992) *Appl. Magn. Reson. 3*, 353.
28. Thurnauer, M. C., and Gast, P. (1985) *Photobiochem. Photobiophys. 9*, 29.
29. van der Est, A., Prisner, T., Bittl, R., Fromme, P., Lubitz, W., Möbius, K., and Stehlik, D. (1997) *J. Phys. Chem. 101*, 1437.
30. Stehlik, D., Bock, C. H., and Peterson, J. (1989) *J. Phys. Chem. 93*, 1612.
31. Füchsle, G., Bittl, R., van der Est, A., Lubitz, W., and Stehlik, D. (1993) *Biochim. Biophys. Acta 1142*, 23.
32. Kothe, G., Weber, S., Ohmes, E., Thurnauer, M. C., and Norris, J. R. (1994) *J. Phys. Chem. 98*, 2706.
33. Weber, S., Ohmes, E., Thurnauer, M. C., Norris, J. R., and Kothe, G. (1995) *Proc. Natl. Acad. Sci. U.S.A. 92*, 7789.
34. Ermler, U., Fritzsch, G., Buchanan, S. K., and Michel, H. (1994) *Structure 2*, 925.
35. Nitschke, W., and Rutherford, A. W. (1991) *Trends Biochem. Sci. 16*, 241.
36. Bittl, R., and Zech, S. (1997) *J. Phys. Chem. 101*, 1429.
37. Nitschke, W., Mattioli, T. A., and Rutherford, A. W. (1996) The FeS-Type Photosystems and the Evolution of Photosynthetic Reaction Centers, in *Origin and Evolution of Biological Energy Conservation* (Baltscheffsky, H., Ed.) pp 177−203, VCH Publishers, New York.
38. Un, S., Atta, M., Fontecave, M., and Rutherford, A. W. (1995) *J. Am. Chem. Soc. 117*, 10713.

BI971097D